THE JOURNAL OF PHYSICAL CHEMISTRY B

Article

pubs.acs.org/JPCB

Chiral Recognition of Amino Acid Enantiomers by a Crown Ether: Chiroptical IR-VCD Response and Computational Study

Juan Ramón Avilés-Moreno,*[,†] María Mar Quesada-Moreno,[†] Juan Jesús López-González,[†] and Bruno Martínez-Haya*[,‡]

[†]Department of Physical and Analytical Chemistry, Campus Las Lagunillas, University of Jaén, E-23071 Jaén, Spain

[‡]Department of Physical, Chemical and Natural Systems, Universidad Pablo de Olavide, E-41013 Seville, Spain

ABSTRACT: We report on a combined experimental and computational study of the chiral recognition of the amino acid serine in protonated form (L/D-SerH$^+$), by the crown ether (*all-S*)-(18-crown-6)-2,3,11,12-tetracarboxylic acid (*S*-18c6H$_4$). Infrared and vibrational circular dichroism spectroscopies (IR-VCD) are employed to characterize the chiroptical response of the complexes formed by *S*-18c6H$_4$ with the L-SerH$^+$ and D-SerH$^+$ enantiomers in dried thin films obtained from aqueous solutions. The study focuses on vibrational modes directly related to the intermolecular hydrogen bonds between the crown ether derivative and serine, responsible for crown−serine binding, namely, the C═O and C—O stretching modes, and on the C—O—H bending mode, which yield intense IR and VCD signals in the range of wavenumbers 900−2000 cm^{-1}. The experimental spectra are analyzed in combination with a computational structural survey and optimization at different levels of density functional theory. The conformational landscape of the complexes is found to be primarily governed by a bowl-like structure of the crown ether host and a tripodal coordination of the protonated R-NH$_3^+$ group of serine with the oxygen atoms of the central ether ring. Additionally, one or two of the carboxylic side groups of the crown ether interact with the −COH and −COOH groups of serine. Chiral selectivity is probed by recording the IR and VCD spectra of dried thin films obtained from aqueous solutions with equimolar concentrations of the two serine enantiomers and the macrocycle. The results demonstrate a marked chiral recognition of L-SerH$^+$ relative to D-SerH$^+$ by the *S*-18c6H$_4$ substrate, which arises from the favorable host−guest coordination through H-bonds at optimum distances and collinear orientations, also involving a limited distortion of the crown ether backbone.

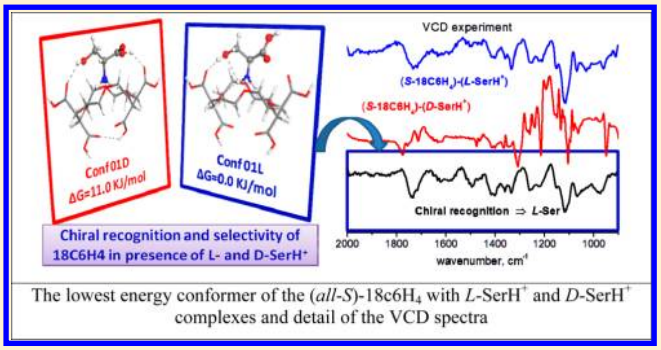

The lowest energy conformer of the (*all-S*)-18c6H$_4$ with *L*-SerH$^+$ and *D*-SerH$^+$ complexes and detail of the VCD spectra

1. INTRODUCTION

Crown ethers have played a leading role in the development of Supramolecular Chemistry during the past decades.[1−3] The importance of crown ethers can be largely attributed to their ability to form inclusion complexes with cationic species, in particular protonated primary and secondary amines.[4−11] This property has motivated a large body of work devoted to the design of chiral substituted crown ethers, mainly for applications in asymmetric separation with electrophoresis[4,5] and high performance liquid chromatography.[6−8]

Most chiral crown ethers investigated to date are based on the (18-crown-6)-2,3,11,12-tetracarboxylic acid. The (*all S*-) enantiomer, relevant to this work (henceforth, *S*-18c6H$_4$), is represented in Figure 1. Previous studies have investigated the structure of 18c6H$_4$ and of its noncovalent complexes with various guest cations (chiral or not) by means of mass spectrometry,[9] infrared spectroscopy,[10] X-ray Diffraction,[11,12] Nuclear Magnetic Resonance,[13−17] and further spectroscopic methods, in particular Electronic Circular Dichroism.[18−20] Recently, the conformational landscape of the free *S*-18c6H$_4$ molecule was investigated in our group with infrared and Vibrational Circular Dichroism (IR-VCD) spectroscopies in combination with quantum chemical calculations.[21] That work provided a detailed analysis of the intramolecular hydrogen bonds sustaining the low-energy conformers of the crown ether in a weakly interacting solvent. In the 18c6H$_4$ molecule, H-

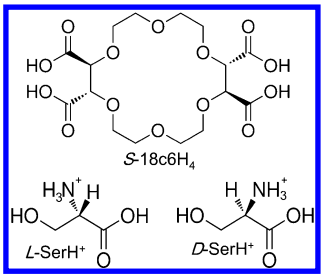

Figure 1. Schematic representation of the host and guest molecules investigated in this work: (*all-S*)-(18-crown-6)-2,3,11,12-tetracarboxylic acid (referred to as *S*-18c6H$_4$ throughout the paper) and protonated serine (denoted L/D-SerH$^+$).

Received: May 22, 2013
Revised: July 10, 2013

   dx.doi.org/10.1021/jp405027s | *J. Phys. Chem. B* XXXX, XXX, XXX−XXX

bonding may take place between pairs of carboxylic groups or between one carboxylic group and one oxygen atom of the ether ring. These interactions produce two types of general structures, namely concave bowl-like or funnel-like configurations in which one of the faces of the macrocyle is more broadly open and exposed to the environment, and barrel-like configurations with more symmetric features on both sides of the crown ring. Such conformations are necessarily altered in the complexation processes investigated in the present work.

Infrared vibrational circular dichroism spectroscopy constitutes a powerful tool for studying the chirality of molecular species and supramolecular organizations, both in solution[22−25] and in the solid phase.[26−30] In the present work, the application of IR and VCD spectroscopies is extended to the investigation of the complexes formed by *S*-18c6H$_4$ with the enantiomers of a primary amine (the amino acid serine in protonated form). Some of the fundamental issues to be addressed are the following: (i) the overall ability of the VCD technique to discern between the complexes formed by the two enantiomers, (ii) the predominant interactions and conformations of the crown−serine complexes, and (iii) the selective binding of the crown ether to any one of the enantiomers of serine, leading to chiral recognition.

The protonated amino acid serine (L/D-SerH$^+$, represented in Figure 1) was chosen as the benchmark guest molecule in this study for different reasons. Serine constitutes a key building block for materials in asymmetric catalysis and enantiomeric separation. Its structure displays three polar groups (COH, COOH, and NH_3^+) rendering a rich framework for intermolecular H-bonding interaction with the crown host. Chiral recognition of serine enantiomers by 18c6H$_4$ has been proposed from a range of experimental studies[11,16−20] and we intend to provide insights into the microscopic conformational background assisting the selective binding process. Finally, the serine amino acid has been characterized both in aqueous solutions and in the solid phase at different pH by IR-VCD spectroscopies and theoretical calculations.[31−33] Hence, the (L/D-SerH$^+$)-(*S*-18c6H$_4$) system constitutes a valuable benchmark system for future developments in the field of chiral recognition.

2. METHODOLOGY

2.1. Experimental Method. (*all-S*)-(18-Crown-6)-2,3,11,12-tetracarboxylic acid (97% purity), L-serine (99% purity), and D-serine (99% purity) were purchased from Sigma-Aldrich and used without further purification. Equimolar solutions (0.057 M) of *S*-18c6H$_4$ and one or both of the two enantiomers, L-serine or D-serine, were prepared in doubly distilled water in order to obtain IR and VCD spectra. HCl was added to ensure a neutral form of the carboxylic side groups of the crown ether and protonation of the serine guest. The spectra were obtained with a JASCO FVS-4000 FTIR spectrometer equipped with a MCT detector (mercury−carbon−telluride, 2000−900 cm^{-1}). Dried thin films obtained from aqueous solutions were prepared on a KCl sample cell.[34] The spectral resolution was set to 4−8 cm^{-1} and 2000−16000 scans, by blocks of 2000 scans, were typically accumulated. For the baseline correction, the spectrum of the film support was subtracted from the thin film spectra.[35,36] Special attention is needed when working with solid samples and thin films in circular dichroism spectroscopy.[37−39] To rule out the presence of spurious peaks in the recorded VCD spectra, the measurements were repeated with the sample cell rotated 90° and 180° around the beam propagation axis, and also with the sample cell flipped to probe the thin film from both of its faces.

2.2. Computational Method. An extensive conformational search was performed for the isolated (*S*-18c6H$_4$)-(L/D-serine) complexes by means of Simulated Annealing with the PCFF force field as implemented in the Materials Studio package.[40] The 20 most stable nonredundant conformers produced with this approach were optimized with density functional theory with the B3LYP functional and the 6-31+G(d) basis set. Finally, the 10 lowest conformers, spanning an energy range of ca. 50 kJ mol^{-1}, were selected for further optimization of the structures and calculation of their relative energies at the M062X/6-311++G(d,p) level. Both B3LYP and M062X calculations have been made within the isolated molecule approach. A set of specific computations were conducted in order to confirm the effect of the chirality of serine on the low-energy conformations obtained thus. For this purpose, new initial conformations were produced from the equilibrium structures obtained by changing the chirality of serine, while keeping the crown substrate unchanged. The subsequent optimization led in all cases to complexes with significantly different structures and energies, indicating that the chirality of the guest plays a key role in this system. Additionally, for the most stable geometries of each complex, potential solvent (water) effects were tested by using IEF-PCM formalism[41] as implemented in Gaussian09. The energies presented throughout the paper are Gibbs free energies, calculated as the sum of electronic energies plus thermal entropy contributions. In any case, the stability ranking of the conformers considered in this work was not altered if electronic energies or enthalpies were considered instead.

To study the charge transfer in the intermolecular hydrogen bonds formed in each complex, a natural bond orbital (NBO) analysis[42] was performed at the B3LYP/6-31+G(d) level of theory. The computational VCD spectrum of each conformer was generated within the framework of Stephens' theory,[43] implemented in Gaussian 09 package[44] and with the aid of the MakeVCD software (JASCO Inc.).[45] For comparison with experiment and assignment of the observed IR and VCD bands, the frequency scaling factors 0.964 (B3LYP) and 0.940 (M062X) were applied to the computed frequencies, in consonance with the recommendation of the NIST database.[46]

3. RESULTS AND DISCUSSION

3.1. Low-Energy Conformers of the Complexes. Our initial computational strategy was to test the influence of two different DFT functionals, namely B3LYP and M062X, in the prediction of the most stable conformers. The M062X functional is a high nonlocality functional with double the amount of nonlocal exchange (2X). It is parametrized for nonmetals and, in contrast with the popular B3LYP functional, it contains a treatment for noncovalent interactions. Previous thorough studies of H-bonded and charge-transfer complexes spanning a large set of functionals suggest that the M062X functional is a good choice in terms of accuracy/cost.[26,31,47,48]

The four carboxylic arms of 18c6H$_4$ are responsible for the chiral character of the molecule and their orientational freedom leads to the rich conformational landscape that drives its complexation behavior. The relevance of the intramolecular H-bonding built by the carboxylic groups for the stabilization of bowl-like or barrel-like conformations in the molecule has already been stressed above.[21] During any complexation process, the intramolecular H-bonding must necessarily be

dx.doi.org/10.1021/jp405027s | J. Phys. Chem. B XXXX, XXX, XXX−XXX

disrupted. Nevertheless, previous experiments based on IR and VCD spectroscopies,[21] X-ray diffraction, and NMR methods[11] have shown that the bowl-like and barrel-like arrangements retain their importance in the complexes of 18c6H$_4$ with primary amines, or with simpler but important cations such as H_3O^+ or NH_4^+.

Figure 2 depicts the three most stable conformers found in our computations for the *S*-18c6H$_4$ complexes with L-SerH$^+$

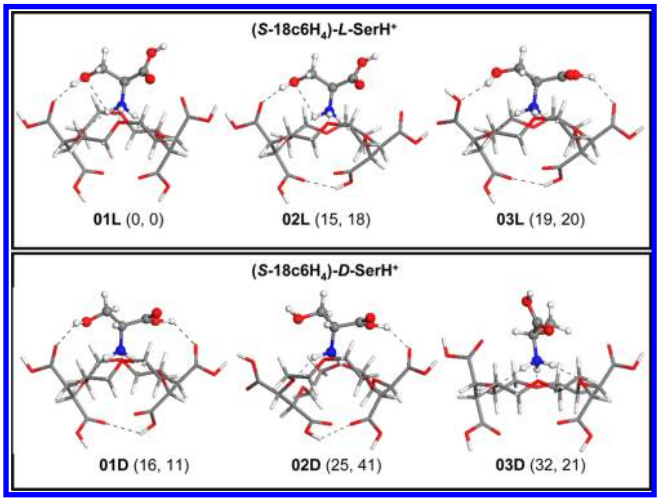

Figure 2. Representation of the three lowest energy conformers of the *S*-18c6H$_4$ complexes with L-SerH$^+$ (denoted **01L**, **02L**, **03L**) and D-SerH$^+$ (denoted **01D**, **02D**, **03D**). The relative free energies predicted by the B3LYP/6-31+G* and M062X/6-311++G(d,p) levels of theory for each type of complex are indicated in parentheses (in kJ mol^{-1}). The **01L** conformer is more stable than the **01D** one by 16 and 11 kJ mol^{-1} at those levels of theory, respectively, indicating a preference of the crown ether substrate to bind the L-SerH$^+$ enantiomer.

and D-SerH$^+$. The free energies of the conformers are indicated with respect to the overall most stable complex, namely the one denoted **01L**, formed by L-SerH$^+$. The lowest energy conformation for D-SerH$^+$, **01D**, is predicted to have a free energy greater than **01L** by 16 (B3LYP) or 11 kJ mol^{-1} (M062X), which indicates a preference of the *S*-18c6H$_4$ substrate for the L-enantiomer.

The three structures shown in Figure 2 span relative conformational free energies for each enantiomer up to ca. 20−30 kJ mol^{-1} and capture the key structural features defining the conformational landscape of the system. The most stable conformers, **01L** and **01D**, lie significantly lower in energy than any other qualitatively different conformer of their kind found in our study. It must be mentioned that we found an ensemble of close lying conformations (within <2 kJ mol^{-1} of **01L** and **01D**), resulting from slight backbone distortions or from rotations of weakly interacting side groups in these conformers. However, such conformers do not introduce any new structural features and lead to insignificant spectral changes and, hence, are not considered in this discussion. It will be shown below that the **01L** and **01D** conformers suffice to interpret the IR and VCD spectra measured for the complexes of each enantiomeric species.

All the low-energy conformers shown in Figure 2 have in common a docking of the protonated serine by means of a tripodal coordination of the R-NH_3^+ protonated amine group with the oxygen atoms of the central ether ring. It is nevertheless worth mentioning that in some higher lying conformers (>30 kJ mol^{-1}, above **01L** or **01D**, not shown) one of the N−H bonds of the amino group interacts instead with one carboxylic side chain of the substrate.

For the two most stable geometries of each complex (**01L** and **01D**), a test for the solvent (water) effect was carried out by using the IEF-PCM formalism at the B3LYP/6-31+G(d) level of theory. The results in terms of structure and relative energy were similar in comparison with the isolated molecule approach just described.

It is interesting to notice that the conformers **02L** and **03L** incorporate additional H-bonds into the complex with respect to the **01L** conformer. In conformer **02L**, the lower carboxylic groups of the substrate are H-bonded with each other, thereby reinforcing the bowl-like shape of the substrate. In conformer **03L**, the carboxylic group of the L-serine is H-bonded to the neighboring carboxylic group of *S*-18c6H$_4$. The incorporation of each of these two H-bonds results in an overall increase in the free energy of the complex by ca. 15 kJ mol^{-1}. While this finding was somewhat unexpected, it is in line with the result of previous studies of 18c6H$_4$−NH_4^+ complexes, where it was realized that the most stable molecular configurations were not necessarily those involving a greater number of intramolecular and/or intermolecular H-bonds.[11] This trend is related to two main facts that are discussed below in some detail: (i) H-bond formation implies some degree of distortion of the crown ether ring and side arms, as well as serine; and (ii) the formation of multiple H-bonds typically implies less favorable OH···O angles and interaction distances in each of the bonds.

Conformer **01D** displays about the maximum number of inter- and intramolecular H-bonds that may be formed in the complex, in a qualitatively similar way as described above for conformer **03L**. Once again, the extensive H-bonding does not lead to more favorable energetic situation in comparison with the **01L** conformation. A specific test computation demonstrated that replacing L-SerH$^+$ with D-SerH$^+$ in conformer **01L** (by reorienting the C−H and the C−COOH bonds on the α-carbon while leaving the rest of the complex unchanged) led after equilibration to conformation **01D**. Conformer **01D** turns out to be particularly stable for the (*S*-18c6H$_4$)-(D-SerH$^+$) complex. The relaxation of the H-bonds leading to conformers **02D** and **03D** is in this case actually energetically unfavorable.

The different trends found for the complexes of the two serine enantiomers demonstrate that the balance between optimum H-bonding and distortion of the structures of the crown substrate and the serine molecule upon complexation is actually quite subtle. This realization motivated the confirmation of the present results by means of a particularly careful survey of the conformational landscape of the complexes performed in the present study with the two different functionals, B3LYP and M062X.

3.2. Geometry and Charge Transfer in the Host−Guest Intermolecular H-Bonds. A NBO analysis was carried out to obtain a detailed insight into the coupling of the N−H and O−H bonds of serine with the oxygen atoms from the ring-ether and the carboxylic groups of the crown, respectively. The calculation involved the six conformers displayed in Figure 2, but we will describe here the results for the most stable complex of each chiral kind, **01L** and **01D**, as they are representative of the overall findings derived from the analysis. The first general conclusion of the NBO analysis is that both of these complexes display host−guest interactions with 98.5% of Lewis structure and 1.5% of non-Lewis structure. These values reflect an appreciable degree of charge delocalization in the

dx.doi.org/10.1021/jp405027s | J. Phys. Chem. B XXXX, XXX, XXX−XXX

intermolecular coordination bonds that stabilize the complexes. The NBO and geometrical analysis outlined below clearly indicates that the greater stability of the (*S*-18c6H$_4$)-(L-SerH$^+$) complex relative to (*S*-18c6H$_4$)-(D-SerH$^+$) is mainly the consequence of the favorable H-bonding of the NH_3^+ and COH sites of the L-serine enantiomer with the crown ether. Some specific features of the charge transfer taking place along the NH···O and OH···O H-bonds in each of the complexes are illustrated in Figure 3 and described in the following paragraphs.

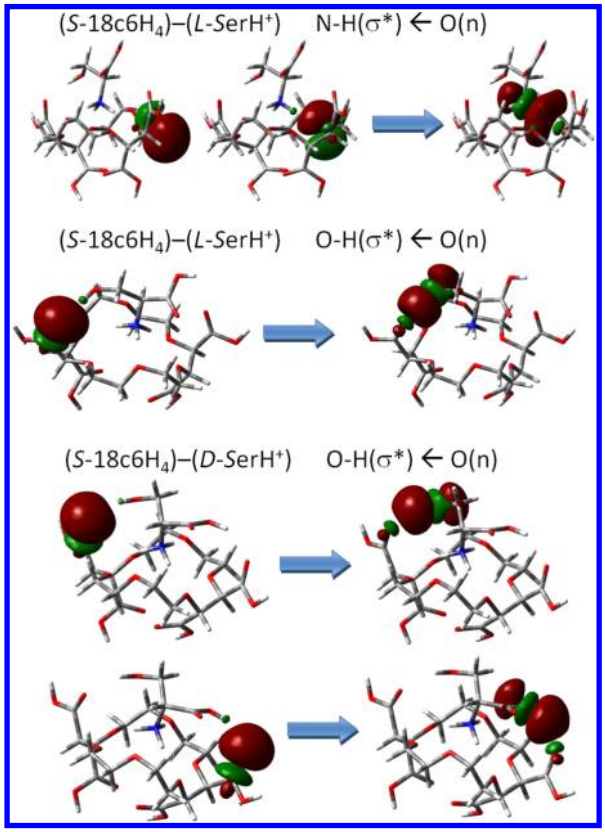

Figure 3. NBOs involved in the charge transfer along typical intermolecular crown−serine H-bonds formed in the **01L** and **01D** complexes at the B3LYP/6-31+G* level of theory. The H-bonds of the **01L** conformer have more favorable geometries and charge transfer than those of the **01D** conformer, which explains the preferential binding of L-SerH$^+$ by the *S*-18c6H$_4$ crown ether. See text for details.

In both the **01L** and **01D** conformers there is a significant charge transfer in the three bonds formed between the NH_3^+ group of L-SerH$^+$ and the oxygen atoms of the crown ether ring. Efficient charge transfer occurs from the lone pairs of the oxygen atom to the σ^* antibonding orbital of the N−H bond, as illustrated in Figure 3. The NH···O coordination is overall more favorable in conformer **01L** relative to **01D**. Conformer **01L** displays three roughly collinear NH···O bonds (bond angle ca. 170°) with bond distances 1.95, 1.95, and 2.21 Å and NBO estimated interaction energies of ca. 40, 40, and 20 kJ mol^{-1}, respectively. In conformer **01D**, two H-bonds are close to collinear (170°) but have different H···O distances, namely 1.88 and 2.05 Å. The third H-bond deviates from linearity (152°, 2.05 Å) and is partly shared by a second oxygen atom (118°, 2.40 Å) in a bifurcated H-bond arrangement. The interaction energies for these bonds are 50, 25, and 20 kJ mol^{-1}, respectively.

The charge transfer associated with the H-bonding between the serine OH sites and the carboxylic groups of the crown ether also shows appreciable differences between the **01L** and **01D** conformers. In both cases, charge transfer takes place between the lone pair of crown-ether oxygen and the σ^* orbital of the serine O−H bond. However, the interaction energy is significantly higher in the single H-bond of the **01L** conformer, namely of 35 kJ mol^{-1} in comparison to 15 kJ mol^{-1} in each of the H-bonds of the **01D** conformer. Figure 3 shows that charge transfer is indeed more efficient in the H-bond of the **01L** conformation as a result of a more collinear and tighter OH···O coordination (170°, 1.88 Å) than any of the two H-bonds in conformer **01D** (136°, 2.00 Å, and 140°, 2.05 Å for the H-bonds formed by the COH and the COOH ends of serine, respectively).

3.3. Chiroptical Response of the (*S*-18c6H$_4$)-(L/D-SerH$^+$) Complexes. Figures 4 and 5 represent the IR and VCD spectra of the complexes formed by (*S*-18c6H$_4$) with L-SerH$^+$ and D-SerH$^+$, respectively. The measurements were recorded on dried thin films obtained from aqueous solutions and containing equimolar fractions of the host and either one of the serine enantiomers. The spectra can be unequivocally attributed to the complex, since the spectra measured for the individual host and guest molecules (also shown in the figures for direct comparison) display appreciable differences. Moreover, panels c and d of Figures 4 and 5 show the artificial IR and VCD spectra, respectively, obtained from both the sum of the SerH$^+$ and *S*-18c6H$_4$ IR-VCD spectra, in equimolar amount, and the difference IR-VCD spectra calculated as the complex IR-VCD signals minus the SerH$^+$ or *S*-18c6H$_4$ IR-VCD signals.

The experimental spectra are represented along with the corresponding spectra predicted by the B3LYP/6-31+G* and M062X/6-311++G(d,p) computations for the most stable conformers of the complexes (**01L** or **01D**). The theoretical spectra were taken as reference to interpret the band structure of the experimental spectra, leading to the schematic vibrational assignment indicated in Figures 4 and 5. The most representative regions recognized in the IR and VCD spectra are related to the C═O stretching (1800−1600 cm^{-1}), C—O—H bending (1400−1100 cm^{-1}), and C—O stretching (1200−950 cm^{-1}) modes, with eventual coupling involving the CH_2 and CH wagging and rocking normal modes.

Figure 4 illustrates the analysis for the (*S*-18c6H$_4$)-(L-SerH$^+$) complex. The main spectral IR-VCD features are highlighted as follows:

(i) Beginning from the high wavenumber range, the C═O stretching band appears centered at ca. 1740 cm^{-1} (broad band) in the IR spectrum, and displays a sequence of (+,−) couplet at 1785 and 1726 cm^{-1} in the VCD spectrum, in good agreement with the corresponding spectra predicted by the computations for the **01L** conformer. The first (+) VCD band can be assigned to the C═O stretching of the four COOH groups of crown and the one of serine moiety. On the contrary, the (−) VCD band could be assigned to the C═O stretching of the four COOH groups of crown.

(ii) Two further weak bands at 1590 and 1490 cm^{-1} in the IR spectrum, which do not display a measurable VCD response, with the exception of the (−) feature at 1500 cm^{-1}, could be assigned to the asymmetric and symmetric NH_3^+ bending modes, respectively.

(iii) The (+,−,−,+,−,+) VCD bands that follow at 1380, 1358, 1331, 1287, 1248, and 1171 cm^{-1} are attributed mainly to

dx.doi.org/10.1021/jp405027s | J. Phys. Chem. B XXXX, XXX, XXX−XXX

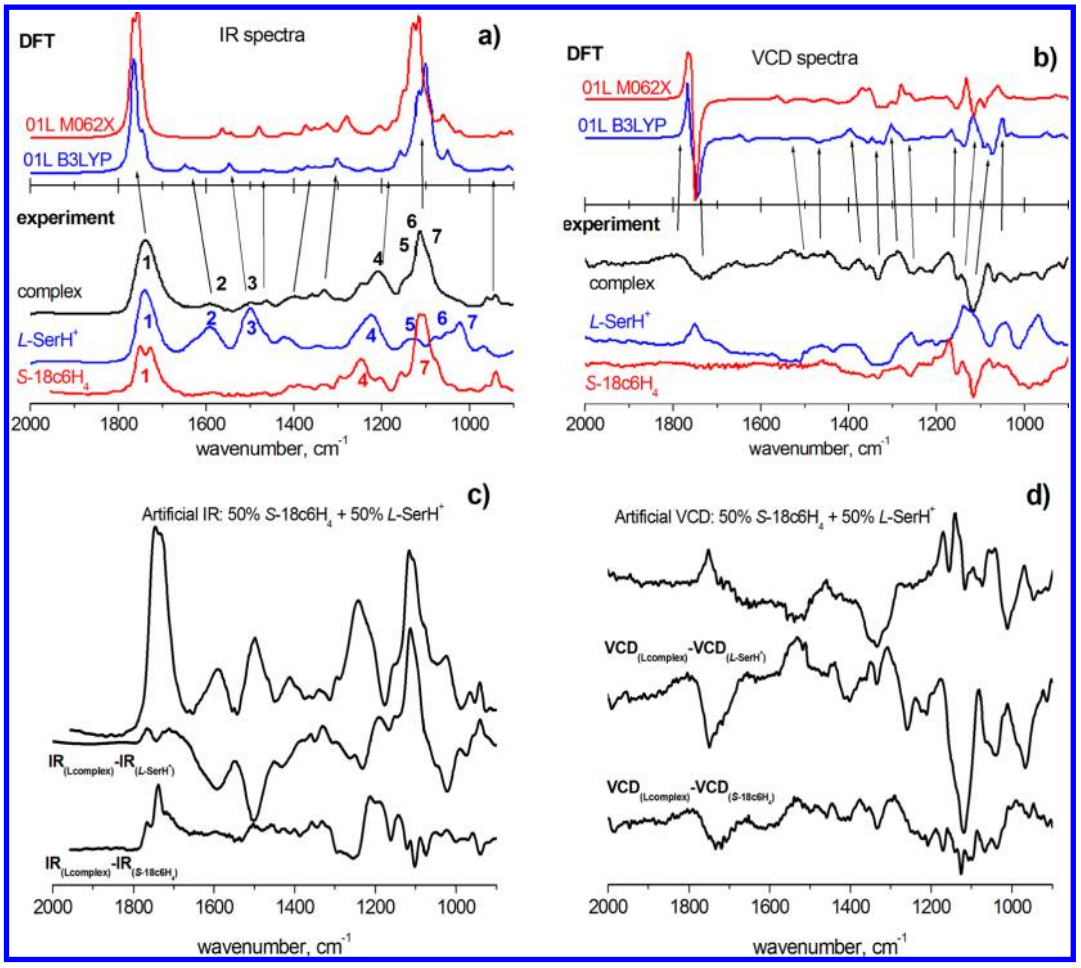

Figure 4. IR (a) and VCD (b) spectra recorded in the C═O stretching, C—O—H bending, and C—O stretching regions for the L-SerH$^+$ and *S*-18c6H$_4$ molecules, and for the (*S*-18c6H$_4$)-(L-SerH$^+$) complex. Panels c and d show the artificial IR and VCD spectra, respectively, obtained from the weighted sum of the L-SerH$^+$ and *S*-18c6H$_4$ IR-VCD spectra, as well as the IR-VCD difference spectra calculated as the complex IR-VCD signals minus the L-SerH$^+$ or *S*-18c6H$_4$ IR-VCD signals. The IR and VCD spectra predicted by the B3LYP/6-31+G* and M062X/6-311++G(d,p) computations for the lowest energy conformer **01L** of the complex are also shown for direct comparison. The bands labeled 1−7 in the IR spectra are related to the following vibrational modes: (1) C═O stretch; (2) asymmetric −NH$_3^+$ bend; (3) symmetric −NH$_3^+$ bend; (4) −COH bend; (5) C−N stretch + CH$_2$ rock; (6) C−N stretch; and (7) C−O stretch.

COH bending vibrations. Both the IR and the VCD experimental spectra are significantly structured in this region, which is well accounted for by the computation. The computations relate the observed structure to the splitting of the COH bending mode into differentiated components related to the concerted vibrations of the carboxylic groups of the crown ether and the amino acid. Those bands can be assigned as follows: (a) the first one to the COH bending vibrations of the serine moiety coupled with the CH$_2$ wagging normal modes; (b) the next four bands to the COH bending vibrations of the four COOH of crown coupled with the CH$_2$ wagging vibrations; and (c) the last one to the COH bending vibrations of the four COOH of crown coupled with the C−O stretchings of crown.

(iv) At lower wavenumbers, the C−O stretching region (1175−950 cm^{-1}) displays a particularly structured series of IR and VCD bands that correlate fairly well with the structure of the computational spectrum. In particular, the (−,−,+,−) VCD bands observed at 1150, 1115, 1081, and 1067 cm^{-1} are theoretically identified as arising mainly from C−O and C−N stretching vibrations of conformer **01L**. The first band (1150 cm^{-1}) is assigned to the C−O stretching vibrations of the crown coupled with the COH bending of crown. The second one (1115 cm^{-1}) belongs to the C−O stretching vibrations of the crown coupled with the CH$_2$ rocking motions. The third one (1081 cm^{-1}) belongs to the C−O stretching of crown coupled with the C−N stretching and CH$_2$ rocking motions. The last band (1067 cm^{-1}) can be assigned to the coupled C−N stretching and CH$_2$ rocking motions. In addition, some relevant information is obtained from panels c and d of Figure 4, where the artificial IR and VCD spectra, built with the contribution of 50% of L-SerH$^+$ and 50% of *S*-18c6H$_4$ are shown to differ from those observed for the L-complex, especially in the C═O, C—O, and C—O—H spectral regions. Moreover, the difference IR-VCD spectra show clearly how the C═O stretching region increases when the complex is formed and how the COH bending region shift to lower frequencies due to the intermolecular H-bonds present in the complex. Finally, the asymmetric and symmetric −NH$_3^+$ bending region decreases in intensity when the complex is formed.

Figure 5 depicts the similar analysis for the (*S*-18c6H$_4$)-(D-SerH$^+$) complex, which shows that the VCD spectra of the two serine enantiomer complexes display distinct signatures that

dx.doi.org/10.1021/jp405027s | J. Phys. Chem. B XXXX, XXX, XXX−XXX

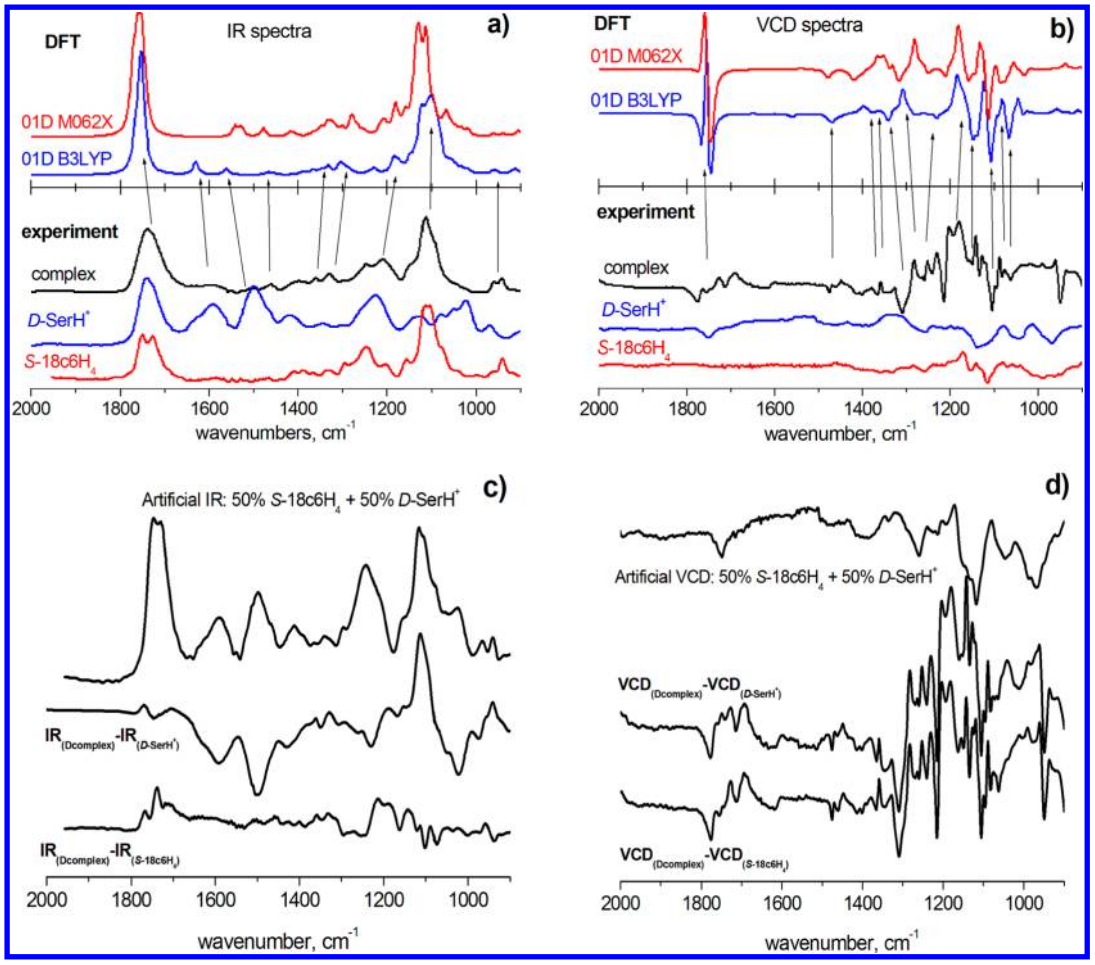

Figure 5. IR (a) and VCD (b) spectra recorded in the C═O stretching, C—O—H bending, and C—O stretching regions for the D-SerH$^+$ and *S*-18c6H$_4$ molecules, and for the (*S*-18c6H$_4$)-(D-SerH$^+$) complex. Panels c and d show the artificial IR and VCD spectra, respectively, obtained from the weighted sum of the D-SerH$^+$ and *S*-18c6H$_4$ IR-VCD spectra, as well as the IR-VCD difference spectra calculated as the complex IR-VCD signals minus the D-SerH$^+$ or *S*-18c6H$_4$ IR-VCD signals. The IR and VCD spectra predicted by the B3LYP/6-31+G* and M062X/6-311++G(d,p) computations for the lowest energy conformer **01D** of the complex are also shown for direct comparison.

differentiate them from each other. The main ones of those IR-VCD signatures are highlighted as follows:

(i) In the C═O stretching region, the experimental VCD data display a structured sequence of (−,+,−,+,−,+) bands at 1773, 1763, 1742, 1728, 1711, and 1692 cm^{-1} assigned to the C═O stretching of the four COOH groups of crown and the one of serine moiety, in good agreement with **01D** structure, instead of the (+,−) bands shown by the (*S*-18c6H4)-(L-SerH$^+$) complex.

(ii) Similar features as those detected for the L-complex have been found in the NH_3^+ bending region for the D-complex. Two weak bands at 1590 and 1490 cm^{-1} have been observed in the IR spectrum, which do not display a measurable VCD response, with the exception of the (−) feature at 1497 cm^{-1}. Those bands could be assigned to the asymmetric and symetric NH_3^+ bending modes, respectively.

(iii) In the COH bending region, the VCD features are more complex, characterized by the (−,+,−,−,+) bands at 1364, 1354, 1331, 1306, and 1281 cm^{-1}, instead of the simpler (−,−,−,−) pattern displayed by the (*S*-18c6H4)-(L-SerH$^+$) complex. Those bands can be assigned to the COH bending vibrations of the four COOH of crown coupled with the CH_2 wagging vibrations. Moreover, the (+,+) VCD bands at 1204 and 1180 cm^{-1} are assigned to the COH bending vibrations of the serine moiety coupled with the CH_2 and NH_3^+ wagging vibrations.

(iv) In the C−O stretching region, the (*S*-18c6H4)-(D-SerH$^+$) complex shows more intense VCD bands with different structure than those found in the spectrum for (*S*-18c6H4)-(L-SerH$^+$) complex. The (−,−,+,−) VCD bands observed at 1148, 1104, 1080, and 1063 cm^{-1} are identified as arising from conformer **01D** instead of the different (+,−,−,+) pattern observed for the (*S*-18c6H4)-(L-SerH$^+$) complex. The first band (1148 cm^{-1}) is assigned to the C−O stretching and COH bending vibrations of the crown. The second and last bands (1104 and 1063 cm^{-1}) are assigned to the C−O stretching coupled with the COH CH_2 rocking motions of crown. The third one (1080 cm^{-1}) belongs to the C−O stretching vibrations of the serine moiety coupled with the CH_2 rocking motions. In the same way as described above for the L-complex, the artificial IR and VCD spectra, built with the contribution of 50% of D-SerH$^+$ and 50% of *S*-18c6H$_4$, depicted in panels c and d of Figure 5, display features that are quite different from those obtained for the D-complex.

It can be concluded that the VCD technique allows us to discern between the complexes formed by the *S*-18c6H$_4$ substrate with each of the L-SerH$^+$ and D-SerH$^+$ enantiomers. The two complexes present similar IR spectra but distinct VCD

dx.doi.org/10.1021/jp405027s | *J. Phys. Chem. B* XXXX, XXX, XXX−XXX

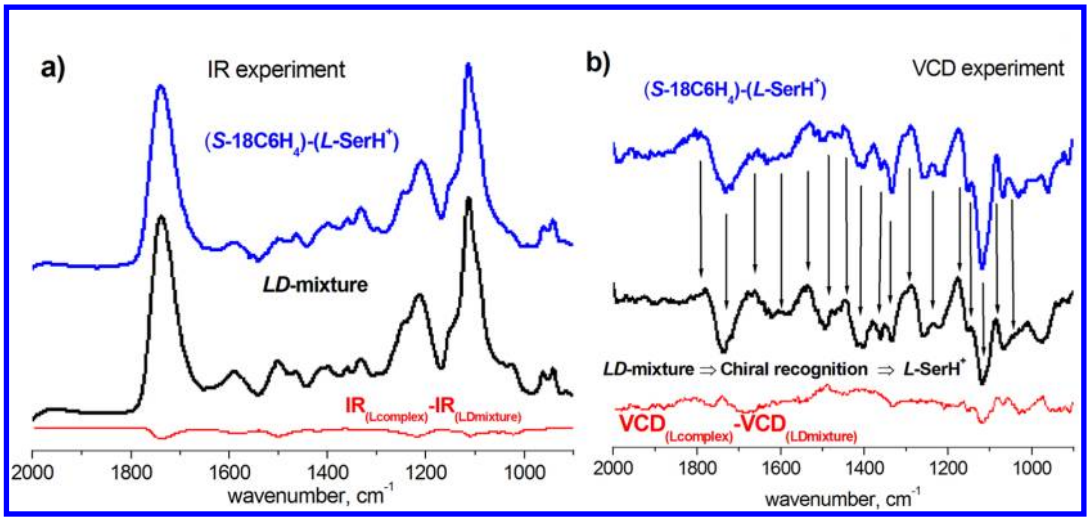

Figure 6. IR (a) and VCD (b) spectra in the C═O stretching, C—O—H bending and C—O stretching regions measured for the (*S*-18c6H$_4$)-(L-SerH$^+$) complex (top traces, in blue), for a sample with equimolar concentrations of the crown ether substrate and the two enantiomers of serine, L- and D-SerH$^+$ (middle trace, in black) and the difference (blue trace minus black trace) IR-VCD spectra (bottom trace, in red). The similarity between both spectra proves that the (*S*-18c6H$_4$) substrate binds preferentially the L-SerH$^+$ enantiomer. The VCD spectrum of the (*S*-18c6H$_4$)-(D-SerH$^+$) displays a clearly different structure (see Figure 5 and text for details).

structural features that are well described by the lowest energy conformers **01L** and **01D**. Based on this result, the next section analyzes the problem of molecular recognition and chiral selectivity of the crown ether upon competitive complexation with the two serine enantiomers.

3.4. Molecular Recognition of L-SerH$^+$ by *S*-18c6H$_4$. To analyze the chiral recognition of L-SerH$^+$ or D-SerH$^+$ by *S*-18c6H$_4$, IR and VCD spectra were recorded on thin films prepared with equimolar amounts of the crown ether and the two serine enantiomers. Figure 6 depicts such spectra and shows that they have close similarity with the corresponding spectra obtained for (*S*-18c6H4)-(L-SerH$^+$) complex, discussed above and shown in Figure 4.

Since the IR spectra of the L-SerH$^+$ and D-SerH$^+$ complexes are similar, both of them are in consonance with the IR spectrum measured for the mixture. Hence, IR spectroscopy by itself does not allow us to discern between the complexes of the two enantiomers. In contrast, the comparison of the corresponding VCD features provides a much clearer evidence for the chiral selectivity of L-SerH$^+$ by *S*-18c6H$_4$. The VCD response obtained from the sample with equimolar amounts of the two enantiomers resembles the (*S*-18c6H$_4$)-(L-SerH$^+$) complex. Specifically, it can be noted in Figure 6 that the sign and position of several VCD features in the C═O stretching, NH_3^+ bending, COH bending, and C—O stretching regions, namely, (i) the (+,−) couplet at 1775 and 1740 cm^{-1}, (ii) the (+) band at 1532 cm^{-1}, and (iii) the (−,−,+,−,−,+) bands at 1250, 1213, 1174, 1142, 1110, and 1087 cm^{-1}, are coincident with the presence of the **01L** complex. As pointed out in Section 3.3, most of these features are absent in the VCD spectrum for the (*S*-18c6H$_4$)-(D-SerH$^+$) complex (see Figure 5).

Finally, Figure 6 shows the difference IR-VCD spectra resulting from the subtraction of the corresponding spectra of the L-complex and of the LD-mixture. The chiral recognition of the L-enantiomer of serine is confirmed from VCD signals, because the residual IR-VCD spectra obtained are almost zero. This proof could be attributed to the same spectral IR-VCD features obtained for the L-complex and LD-mixture.

4. SUMMARY AND CONCLUSIONS

A combination of IR and VCD spectroscopies with quantum chemical computations has been employed to characterize the microscopic framework underlying the chiral recognition of the protonated serine by the crown ether host (*all-S*)-(18-crown-6)-2,3,11,12-tetracarboxylic acid (Figure 1).

The study has been focused on some of the vibrational modes more closely related to the host−guest H-bonding interactions, namely, the C—O and C═O stretching modes, and on the C—O—H bending mode. While the IR spectra of the (*S*-18c6H$_4$)-(L-SerH$^+$) and (*S*-18c6H$_4$)-(D-SerH$^+$) complexes show minor differences from each other, their corresponding VCD spectra display quite distinct features. This finding has allowed us to monitor the chiral recognition of L-SerH$^+$ relative to D-SerH$^+$ by the crown ether: the chiroptical response recorded for a thin film obtained from a solution equimolar in the crown ether and in each of the two serine enantiomers leads to a VCD spectrum resembling the complex of L-SerH$^+$.

The computations performed at different levels of density functional theory (B3LYP and M062X functionals) predict low-energy conformers in which the crown ether maintains a roughly bowl-like shape. The docking of the protonated serine then involves a tripodal coordination of its R-NH_3^+ protonated amine group with the oxygen atoms of the central ether ring, and of its −COH and −COOH end groups with the side carboxylic arms of the crown ether. The most stable theoretical conformations for the complex of each serine enantiomer (**01L** and **01D** in Figure 2) lead to simulated IR and VCD spectra in good agreement with experiments. Importantly, the computation corroborates the preferential binding of L-SerH$^+$ by *S*-18c6H$_4$ and attributes the chiral recognition to the formation of host−guest H-bonds with favorable distances and orientations.

A general contribution of the present study has been the illustration of the potential of the combination of IR-VCD spectroscopies and computational techniques for the elucidation of the conformational landscape of flexible chiral molecules and their H-bonded networks in complexes with specific enantiomeric guests. We hope that this contribution encourages

dx.doi.org/10.1021/jp405027s | J. Phys. Chem. B XXXX, XXX, XXX−XXX

further work in this direction on related inclusion supramolecular systems.

AUTHOR INFORMATION

Corresponding Author

*E-mail: jraviles@ujaen.es (J.R.A.-M.) and bmarhay@upo.es (B.M.-H.).

Notes

The authors declare no competing financial interest.

ACKNOWLEDGMENTS

J.R.A.M. thanks the *Junta de Andalucía* (Spain) for a postdoctoral grant. M.M.Q.M. thanks the University of Jaén for a predoctoral fellowship. Funding was provided by research programmes of *Junta de Andalucía*-FEDER (P08-FQM-4096, P09-FQM-4938) and of the Government of Spain (CTQ2012-32345, CSD2009-00038).

REFERENCES

(1) Pedersen, C. J. The Discovery of Crown Ethers. *Science* **1988**, *241*, 536−540.

(2) Gokel, G. W. *Crown Ethers and Cryptands*; Royal Society of Chemistry: Cambridge, U.K., 1994.

(3) Gawronski, J.; Gawronska, K. *Tartaric and Malic Acids in Synthesis − A Source Book of Building Blocks, Ligands, Auxiliaries, and Resolving Agents*; J. Wiley & Sons: Hoboken, NJ, 1999; Chapter 5.

(4) Kuhn, R. Enantiomeric Separation by Capillary Electrophoresis Using a Crown Ether as Chiral Selector. *Electrophoresis* **1999**, *20*, 2605−2613.

(5) Tanaka, Y.; Otsuka, K.; Terabe, S. Experimental Designs to Investigate Capillary Electrophoresis-Electrospray Ionization-Mass Spectrometry Enantioseparation with the Partial-Filling Technique. *J. Chromatogr., A* **2000**, *875*, 323−330.

(6) Hyun, M. H. Preparation and Application of HPLC Chiral Stationary Phases Based on (+)-(18-Crown-6)-2,3,11,12-tetracarboxylic Acid. *J. Sep. Sci.* **2006**, *29*, 750−761.

(7) Manolescu, C.; Grinberg, M.; Field, C.; Ma, S.; Shen, S.; Lee, H.; Wang, Y.; Granger, A.; Chen, Q.; McCaffrey, J.; et al. Studies of the Interactions of Amino Alcohols Using High Performance Liquid Chromatography with Crown Ether Stationary Phases. *J. Liq. Chromatogr. Relat. Technol.* **2008**, *31*, 2219−2234.

(8) Shen, S.; Ma, S.; Lee, H.; Manolescu, C.; Grinberg, M.; Yee, N.; Senanayake, C.; Grinberg, N. HPLC Enatiomeric Separation of Aromatic Amines Using Crown Ether Tetracarboxylic Acid. *J. Liq. Chromatogr. Relat. Technol.* **2010**, *33*, 153−166.

(9) Gerbaux, P.; De Winter, J.; Cornil, D.; Ravicini, K.; Pesesse, G.; Cornil, J.; Flammang, R. Noncovalent Interactions between ([18]-Crown-6)-Tetracarboxylic Acid and Amino Acids: Electrospray-Ionization Mass Spectrometry Investigation of the Chiral-Recognition Processes. *Chem.—Eur. J.* **2008**, *14*, 11039−11049.

(10) Hurtado, P.; Gámez, F.; Hamad, S.; Martínez−Haya, B.; Steill, J. D.; Oomens, J. Multipodal Coordination of a Tetracarboxylic Crown Ether with NH_4^+: A Vibrational Spectroscopy and Computational Study. *J. Chem. Phys.* **2012**, *136*, 114301−114301−6.

(11) Nagata, H.; Nishi, H.; Kamigauchi, M.; Ishida, T. Guest-dependent Conformation of 18-crown-6 Tetracarboxylic Acid: Relation to Chiral Separation of Racemic Amino Acids. *Chirality* **2008**, *20*, 820−827.

(12) Machida, Y.; Nishi, H.; Nakamura, K. Crystallographic Studies for the Chiral Recognition of the Novel Chiral Stationary Phase Derived from (+)-(R)-18-crown-6 Tetracarboxylic Acid. *Chirality* **1999**, *11*, 173−178.

(13) Machida, Y.; Nakamura, K.; Nishi, H. Nuclear Magnetic Resonance Studies for the Chiral Recognition of (+)-(R)-18-crown-6-tetracarboxylic Acid to Amino Compounds. *J. Pharm. Biomed. Anal.* **2003**, *30*, 1929−1942.

(14) Bang, E.; Jung, J.-W.; Lee, W.; Lee, D. W. Chiral Recognition of (18-crown-6)-tetracarboxylic Acid as a Chiral Selector Determined by NMR Spectroscopy. *J. Chem. Soc., Perkin Trans. 2* **2001**, *9*, 1685−1692.

(15) Lovely, A. E.; Wenzel, T. J. Chiral NMR Discrimination of Amines: Analysis of Secondary, Tertiary, and Prochiral Amines using (18-crown-6)-2,3,11,12-tetracarboxylic Acid. *Chirality* **2008**, *20*, 370−378.

(16) Wenzel, T. J.; Thurston, J. E. Enantiomeric Discrimination in the NMR Spectra of Underivatized Amino Acids and α-methyl Amino Acids using (+)-(18-crown-6)-2,3,11,12-tetracarboxylic Acid. *Tetrahedron Lett.* **2000**, *41*, 3769−3772.

(17) Duddeck, H.; Díaz Gómez, E. Chiral Recognition of Ethers by NMR Spectroscopy. *Chirality* **2009**, *21*, 51−68.

(18) Somogyi, L.; Huszthy, P.; Köntös, Z.; Hollósi, M. Enantiomeric Recognition of Aralkyl Ammonium Salts by Chiral Pyridino-18-crown-6 Ligands: Use of Circular Dichroism Spectroscopy. *Chirality* **1997**, *9*, 545−549.

(19) Farkas, V.; Szalay, L.; Vass, E.; Hollósi, M.; Horváth, G.; Huszthy, P. Probing the Discriminating Power of Chiral Crown Hosts by CD Spectroscopy. *Chirality* **2003**, *15*, S65−S73.

(20) Szarvas, S.; Szalay, L.; Vass, E.; Hollósi, M.; Samu, E.; Huszthy, P. Chiroptical Properties of Cation Complexes of Chiral Phenazino-18-crown-6 Ether-Type Hosts. *Chirality* **2005**, *17*, 345−351.

(21) Avilés Moreno, J. R.; Partal Ureña, F.; López González, J. J.; Gámez, F.; Martínez−Haya, B. Conformational Landscape of a Chiral Crown Ether: a Vibrational Circular Dichroism Spectroscopy and Computational Study. *Tetrahedron: Asymmetry* **2012**, *23*, 294−299.

(22) Partal Ureña, F.; Avilés Moreno, J. R.; López González, J. J. Conformational Flexibility in Terpenes: Vibrational Circular Dichroism (VCD), Infrared and Raman Study of S-(−)-perillaldehyde. *J. Phys. Chem. A* **2008**, *112*, 7887−7893.

(23) Avilés Moreno, J. R.; Partal Ureña, F.; López González, J. J. Conformational Preference of a Chiral Terpene: Vibrational Circular Dichroism (VCD), Infrared and Raman Study of S-(−)-limonene Oxide. *Phys. Chem. Chem. Phys.* **2009**, *11*, 2459−2467.

(24) Partal Ureña, F.; Avilés Moreno, J. R.; López González, J. J. Rotational Strength Sign and Normal Modes Description: A Theoretical and Experimental Comparative Study in Bicyclic Terpenes. *Chirality* **2010**, *22*, E123−E129.

(25) Merten, C.; Hyun, M. H.; Xu, Y. Absolute Configuration and Predominant Conformations of a Chiral Crown Ether-Based Colorimetric Sensor: A Vibrational Circular Dichroism Spectroscopy and DFT Study of Chiral Recognition. *Chirality* **2013**, *25*, 294−300.

(26) Avilés Moreno, J. R.; Quesada Moreno, M. d. M.; Partal Ureña, F.; López González, J. J. Conformational Preference of Short Aromatic Amino Acids from the FT-IR, FT-Raman and Far-IR Spectroscopies, and Quantum Chemical Calculations: L-phenylalanine and L-tyrosine. *Tetrahedron: Asymmetry* **2012**, *23*, 1084−1092.

(27) González, J. J. L.; Ureña, F. P.; Moreno, J. R. A.; Mata, I.; Molins, E.; Claramunt, R. M.; López, C.; Alkorta, I.; Elguero, J. The Chiral Structure of 1*H*-indazoles in the Solid State: a Crystallographic, Vibrational Circular Dichroism and Computational Study. *New J. Chem.* **2012**, *36*, 749−758.

(28) Graus, S.; Tejedor, R. M.; Uriel, S.; Serrano, J. L.; Alkorta, I.; Elguero, J. Crystallization of an Achiral Cyclohexanone Ethylene Ketal in Enantiomorphs and Determination of the Absolute Structure. *J. Am. Chem. Soc.* **2010**, *132*, 7862−7863.

(29) Avilés Moreno, J. R.; López González, J. J.; Partal Ureña, F.; Vera, F.; Ros, M. B.; Sierra, T. Study of the Photoinduced Supramolecular Chirality in Columnar Liquid Crystals by Infrared and VCD Spectroscopies. *J. Phys. Chem. B* **2012**, *116*, 5090−5096.

(30) Tejedor, R. M.; Oriol, L.; Serrano, J. L.; Partal Ureña, F.; López González, J. J. Photoinduced Chiral Nematic Organization in an Achiral Glassy Nematic Azopolymer. *Adv. Funct. Mater.* **2007**, *17*, 3486−3492.

(31) Quesada-Moreno, M. M.; Avilés-Moreno, J. R.; Márquez-García, A. A.; Partal-Ureña, F.; López-González, J. J. L-Serine in Aqueous Solutions at Different pH: Conformational Preferences and Vibra-

tional Spectra of Cationic, Anionic and Zwitterionic Species. *J. Mol. Struct.* **2013**, *1046*, 136−146.
(32) Hernandez, B.; Pflüger, F.; Adenier, A.; Nsangou, M.; Kruglik, S. G.; Ghomi, M. Energy Maps, Side Chain Conformational Flexibility, and Vibrational Features of Polar Amino Acids L-serine and L-threonine in Aqueous Environment. *J. Chem. Phys.* **2011**, *135*, 055101−7.
(33) Zhu, P.; Yang, G.; Poopari, M. R.; Bie, Z.; Xu, Y. Conformations of Serine in Aqueous Solutions as Revealed by Vibrational Circular Dichroism. *ChemPhysChem* **2012**, *13*, 1272−1281.
(34) Real Crystal® IR sample cards. U.S. Patent No. 7,932,095 and UK Patent No. GB2372102.
(35) Shanmugam, G.; Polavarapu, P. L. Film Techniques for Vibrational Circular Dichroism Measurements. *Appl. Spectrosc.* **2005**, *59*, 673−681.
(36) Deplazes, E.; Bronswijk, W.; van Zhu, F.; Barron, L. D.; Ma, S.; Nafie, L. A.; Jalkanen, K. J. A Combined Theoretical and Experimental Study of the Structure and Vibrational Absorption, Vibrational Circular Dichroism, Raman and Raman Optical Activity Spectra of the L-histidine Zwitterion. *Theor. Chem. Acc.* **2008**, *119*, 155−176.
(37) Kuroda, R.; Harada, T.; Shindo, Y. A Solid-State Dedicated Circular Dichroism Spectrophotometer: Development and Application. *Rev. Sci. Instrum.* **2001**, *72*, 3802−3810.
(38) Merten, C.; Kowalik, T.; Hartwig, A. Vibrational Circular Dichroism Spectroscopy of Solid Polymer Films: Effects of Sample Orientation. *Appl. Spectrosc.* **2008**, *62*, 901−905.
(39) Buffeteau, T.; Lagugné-Labarthet, F.; Sourisseau, C. Vibrational Circular Dichroism in General Anisotropic Thin Solid Films: Measurement and Theoretical Approach. *Appl. Spectrosc.* **2005**, *59*, 732−745.
(40) *Accelrys Materials Studio 4.4*; Accelrys, Inc.: San Diego, CA, 2008.
(41) Tomasi, J.; Mennucci, B.; Cammi, R. Quantum Mechanical Continuum Solvation Models. *Chem. Rev.* **2005**, *105*, 2999−3093.
(42) Foster, J. P.; Weinhold, F. Natural Hybrid Orbitals. *J. Am. Chem. Soc.* **1980**, *102*, 7211−7218.
(43) Cheeseman, J. R.; Frisch, M. J.; Devlin, F. J.; Stephens, P. J. Ab Initio Calculation of Atomic Axial Tensors and Vibrational Rotational Strengths using Density Functional Theory. *Chem. Phys. Lett.* **1996**, *252*, 211−220.
(44) Frisch, M. J.; Trucks, G. W.; Schlegel, H. B.; Scuseria, G. E.; Robb, M. A.; Cheeseman, J. R.; Scalmani, G.; Barone, V.; Mennucci, B.; Petersson, G. A.; et al. *GAUSSIAN09*, Revision A.01; Gaussian, Inc.: Wallingford, CT, 2009.
(45) Jasco Spectra Manager for Windows.
(46) NIST Standard Reference Database 101; Computational Chemistry Comparison and Benchmark DataBase: http://cccbdb.nist.gov/vibscalejust.asp.
(47) Steinmann, S. N.; Piemontesi, C.; Delachat, A.; Corminboeuf, C. Why are the Interaction Energies of Charge-Transfer Complexes Challenging for DFT? *J. Chem. Theory Comput.* **2012**, *8*, 1629−1640.
(48) Avilés Moreno, J. R.; Partal Ureña, F.; López González, J. J. Conformational Landscape and Hydrogen Bonding in (*S*)-(−)-Perillyc Acid: Experimental VCD, IR, Raman, and Theoretical DFT Studies. *Tetrahedron: Asymmetry* **2012**, *23*, 780−788.